Verification of the Cardinal Multiphysics Solver

1-D Coupled Heat Transfer and Neutron Transport

Lewis Gross, April Novak, Patrick Shriwise, and Paul Wilson

August 15, 2022

WISCONSIN

UNIVERSITY OF WISCONSIN–MADISON

Outline

Modern Multiphysics Simulation and the Importance of V&V: Cardinal

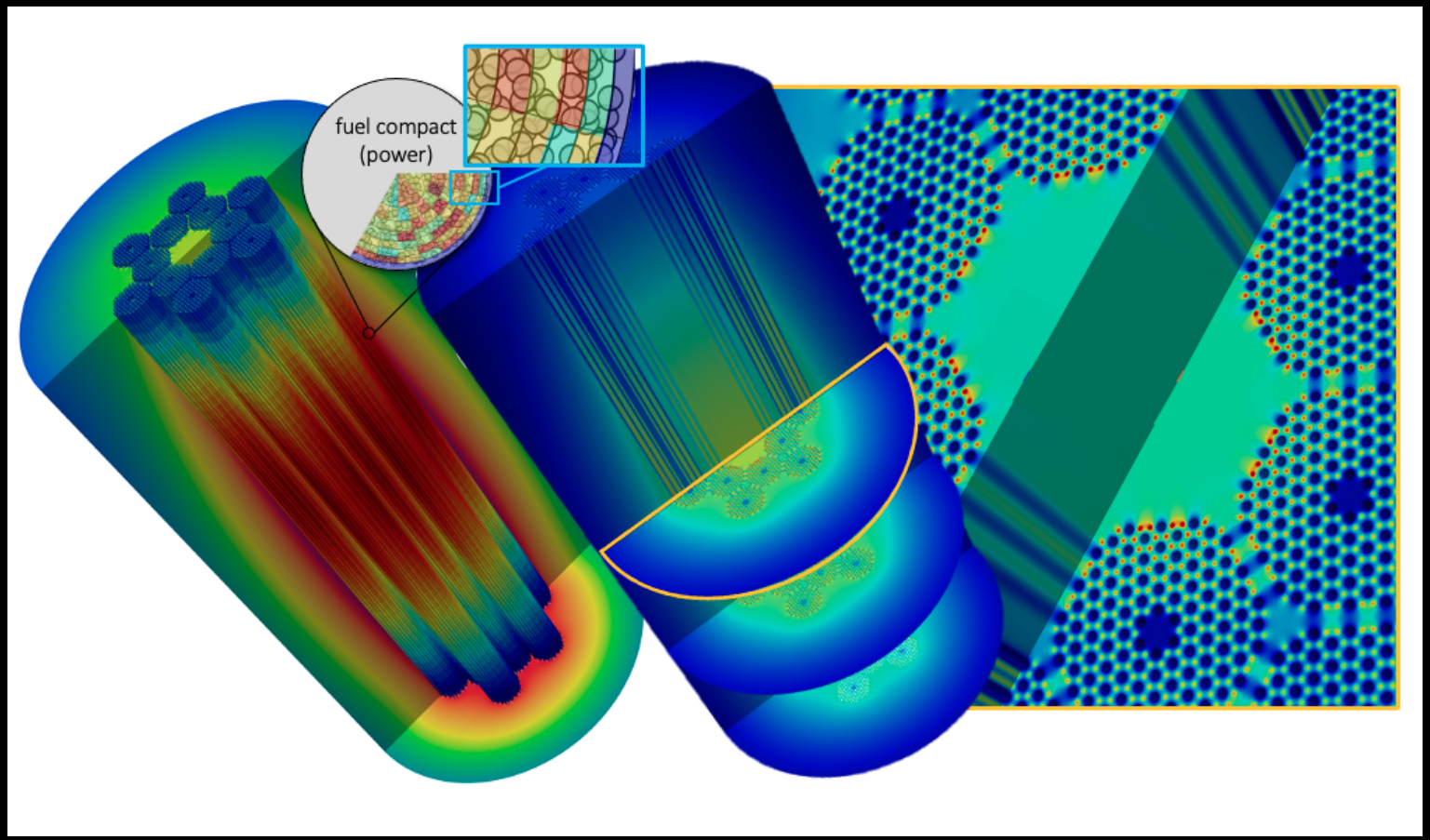

Modern Multiphysics Simulation and the Importance of V&V: Cardinal

Modern Multiphysics Simulation and the Importance of V&V: Cardinal

- Many new emerging tools have great potential, but they require Verification and Validation.

Modern Multiphysics Simulation and the Importance of V&V: Cardinal

- Many new emerging tools have great potential, but they require Verification and Validation.
- Verification via analytical benchmarks allow measurement of true error for a numerical simulation.

Modern Multiphysics Simulation and the Importance of V&V: Cardinal

- Many new emerging tools have great potential, but they require Verification and Validation.
- Verification via analytical benchmarks allow measurement of true error for a numerical simulation.
- Greisheimer and Kooreman 1-D presented an analytical benchmark that features coupled heat transfer and neutron transport [1].

Modern Multiphysics Simulation and the Importance of V&V: Cardinal

- Many new emerging tools have great potential, but they require Verification and Validation.
- Verification via analytical benchmarks allow measurement of true error for a numerical simulation.
- Greisheimer and Kooreman 1-D presented an analytical benchmark that features coupled heat transfer and neutron transport [1].
- Cardinal [2] our software choice to model this benchmark couples OpenMC [3] neutronics and NekRS [4] CFD into the MOOSE framework [5]

Cardinal and MOOSE Framework

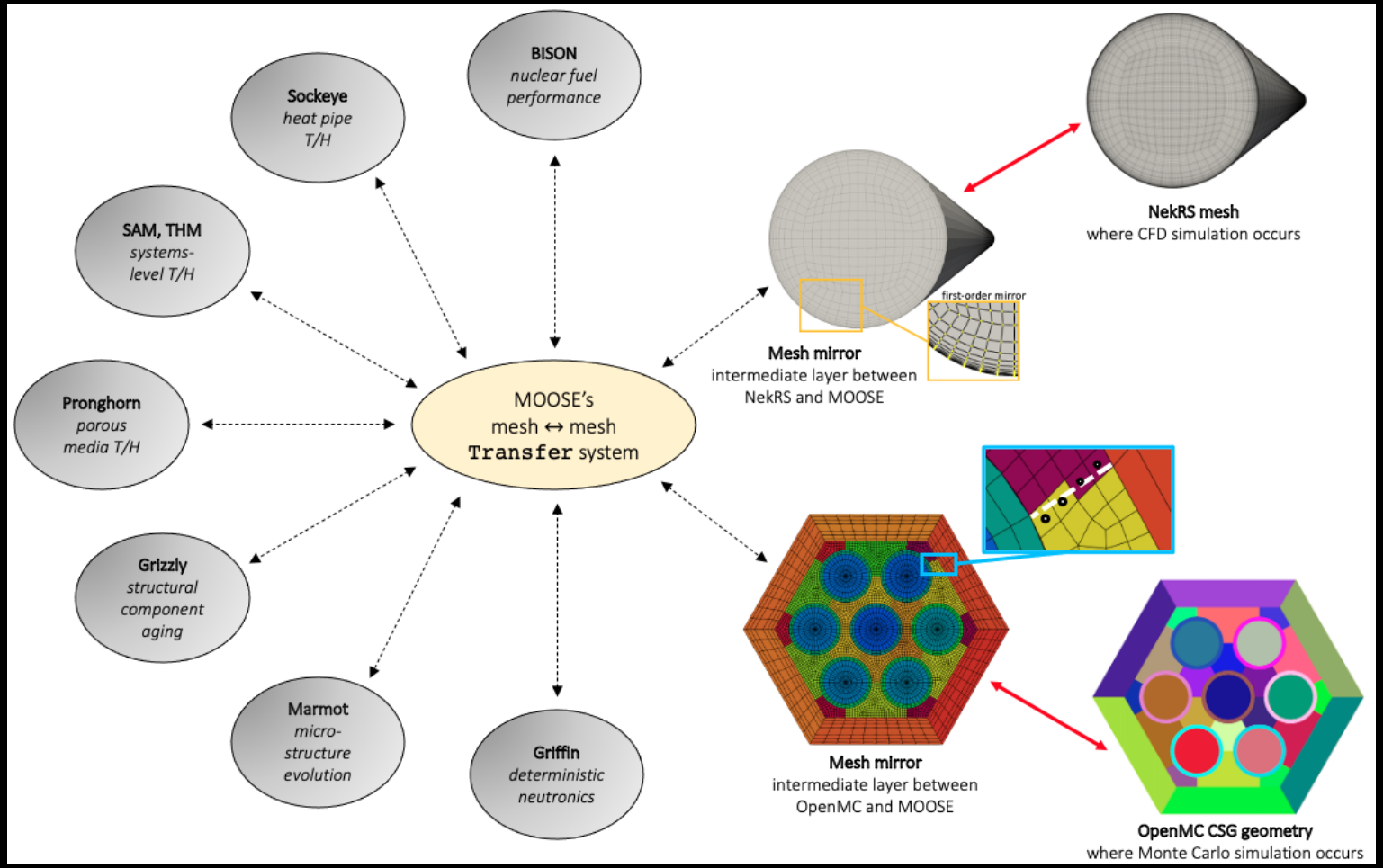

Analytical Benchmark

Analytical Benchmark

- This analytical benchmark includes S_2 transport, Doppler-broadened cross sections, 1-D thermal conduction and expansion, and convective boundary conditions.

Analytical Benchmark

- This analytical benchmark includes S_2 transport, Doppler-broadened cross sections, 1-D thermal conduction and expansion, and convective boundary conditions.
  - S_2 transport restricts particles to move in the $\pm$x direction; or $\mu = \cos\theta = \pm 1$.

Analytical Benchmark

- This analytical benchmark includes S_2 transport, Doppler-broadened cross sections, 1-D thermal conduction and expansion, and convective boundary conditions.
  - S_2 transport restricts particles to move in the $\pm$x direction; or $\mu = \cos\theta = \pm 1$.
  - Doppler-broadening

$$\sigma_t(x) = \sigma_{t,0}\sqrt{\frac{T_0}{T(x)}}. \tag{1}$$

Analytical Benchmark

- This analytical benchmark includes S_2 transport, Doppler-broadened cross sections, 1-D thermal conduction and expansion, and convective boundary conditions.
  - S_2 transport restricts particles to move in the $\pm$x direction; or $\mu = \cos\theta = \pm 1$.
  - Doppler-broadening

$$\sigma_t(x) = \sigma_{t,0}\sqrt{\frac{T_0}{T(x)}}. \tag{1}$$

  - 1-D thermal expansion

$$\rho(x) = \rho_0\sqrt{\frac{T_0}{T(x)}}. \tag{2}$$

Analytical Benchmark

- This analytical benchmark includes S_2 transport, Doppler-broadened cross sections, 1-D thermal conduction and expansion, and convective boundary conditions.
  - S_2 transport restricts particles to move in the $\pm$x direction; or $\mu = \cos\theta = \pm 1$.
  - Doppler-broadening

$$\sigma_t(x) = \sigma_{t,0}\sqrt{\frac{T_0}{T(x)}}. \tag{1}$$

  - 1-D thermal expansion

$$\rho(x) = \rho_0\sqrt{\frac{T_0}{T(x)}}. \tag{2}$$

  - Linear temperature dependence on thermal conductivity

$$\kappa(x) = \kappa_0 T(x) \tag{3}$$

Analytical Benchmark

- This analytical benchmark includes S_2 transport, Doppler-broadened cross sections, 1-D thermal conduction and expansion, and convective boundary conditions.
  - S_2 transport restricts particles to move in the $\pm$x direction; or $\mu = \cos\theta = \pm 1$.
  - Doppler-broadening

$$\sigma_t(x) = \sigma_{t,0}\sqrt{\frac{T_0}{T(x)}}. \tag{1}$$

  - 1-D thermal expansion

$$\rho(x) = \rho_0\sqrt{\frac{T_0}{T(x)}}. \tag{2}$$

  - Linear temperature dependence on thermal conductivity

$$\kappa(x) = \kappa_0 T(x) \tag{3}$$

- The conduction equation governs energy conservation in the slab and can be described in terms of the thermal conductivity κ, the energy released **per reaction** q, the total macroscopic cross section Σ_t, and the neutron flux ϕ,

$$\frac{d}{dx}\left[\kappa(T)\frac{dT(x)}{dx}\right] + q\Sigma_t(x)\phi(x) = 0 \tag{4}$$

Analytical Benchmark

Analytical Benchmark

- Based on 1-D S_2 transport, the neutron flux is governed by

$$\frac{d}{dx}\left[\frac{1}{\Sigma_t(x)}\frac{d\phi(x)}{dx}\right] + \Sigma_t(x)\,(\lambda - 1)\,\phi(x) = 0 \tag{5}$$

Analytical Benchmark

- Based on 1-D S_2 transport, the neutron flux is governed by

$$\frac{d}{dx}\left[\frac{1}{\Sigma_t(x)}\frac{d\phi(x)}{dx}\right] + \Sigma_t(x)\,(\lambda - 1)\,\phi(x) = 0 \tag{5}$$

- where $\lambda \equiv (\frac{1}{k_{eff}}\frac{\nu\Sigma_f}{\Sigma_t} + \frac{\Sigma_s}{\Sigma_t})$ is the combined in-scattering and quasi-static fission source term [1].

Analytical Benchmark

- Based on 1-D S_2 transport, the neutron flux is governed by

$$\frac{d}{dx}\left[\frac{1}{\Sigma_t(x)}\frac{d\phi(x)}{dx}\right] + \Sigma_t(x)\,(\lambda - 1)\,\phi(x) = 0 \tag{5}$$

- where $\lambda \equiv (\frac{1}{k_{eff}}\frac{\nu\Sigma_f}{\Sigma_t} + \frac{\Sigma_s}{\Sigma_t})$ is the combined in-scattering and quasi-static fission source term [1].
- Using (1) and (2) gives a Doppler-broadened, macroscopic, total cross section that accounts for changes in density due to temperature as

$$\begin{aligned}\Sigma_t(x) &= \frac{\rho_0\sigma_{t,0}N_A}{A}\frac{T_0}{T(x)} \\ &= \Sigma_{t,0}\frac{T_0}{T(x)},\end{aligned} \tag{6}$$

Analytical Benchmark

- Based on 1-D S_2 transport, the neutron flux is governed by

$$\frac{d}{dx}\left[\frac{1}{\Sigma_t(x)}\frac{d\phi(x)}{dx}\right] + \Sigma_t(x)\,(\lambda - 1)\,\phi(x) = 0 \tag{5}$$

- where $\lambda \equiv (\frac{1}{k_{eff}}\frac{\nu\Sigma_f}{\Sigma_t} + \frac{\Sigma_s}{\Sigma_t})$ is the combined in-scattering and quasi-static fission source term [1].
- Using (1) and (2) gives a Doppler-broadened, macroscopic, total cross section that accounts for changes in density due to temperature as

$$\begin{aligned}\Sigma_t(x) &= \frac{\rho_0\sigma_{t,0}N_A}{A}\frac{T_0}{T(x)} \\ &= \Sigma_{t,0}\frac{T_0}{T(x)},\end{aligned} \tag{6}$$

- where $\sigma_{t,0}$ is the total microscopic cross section at T_0, N_A is Avogadro's number, and A is the mass number of the medium.

System Domain, Differential Equations, and Boundary Conditions

System Domain, Differential Equations, and Boundary Conditions

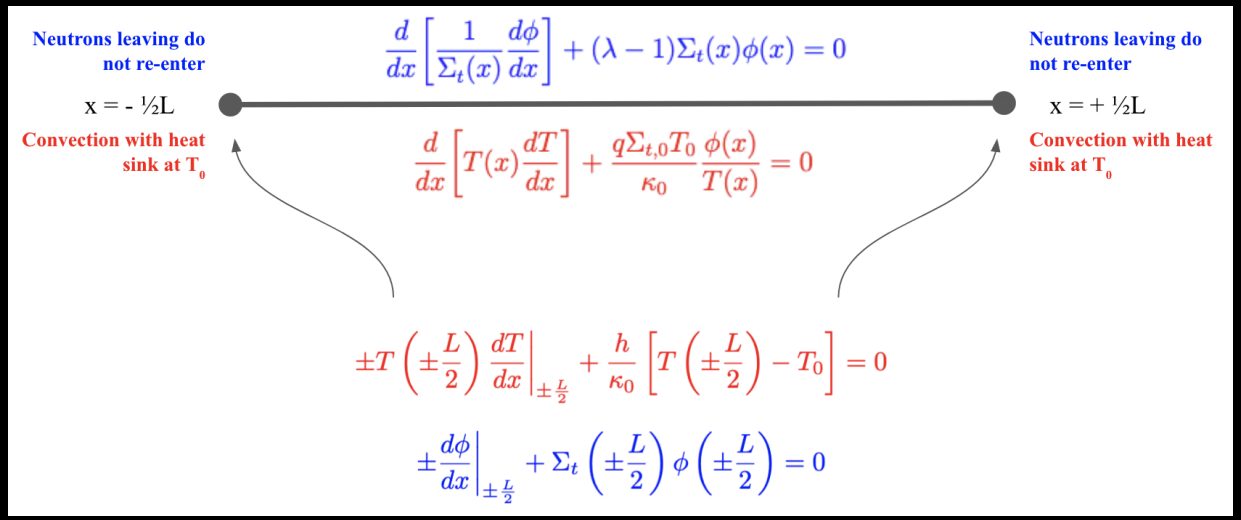

System Domain, Differential Equations, and Boundary Conditions

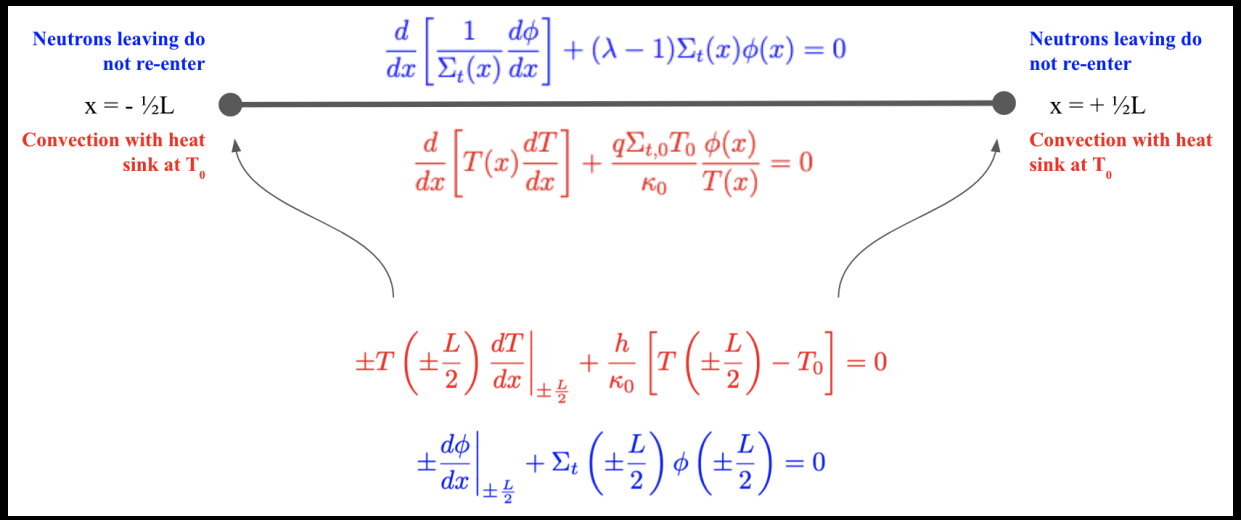

- The fundamental assumption (ansatz) of [1]: $T(x) = f\phi(x)$.

System Domain, Differential Equations, and Boundary Conditions

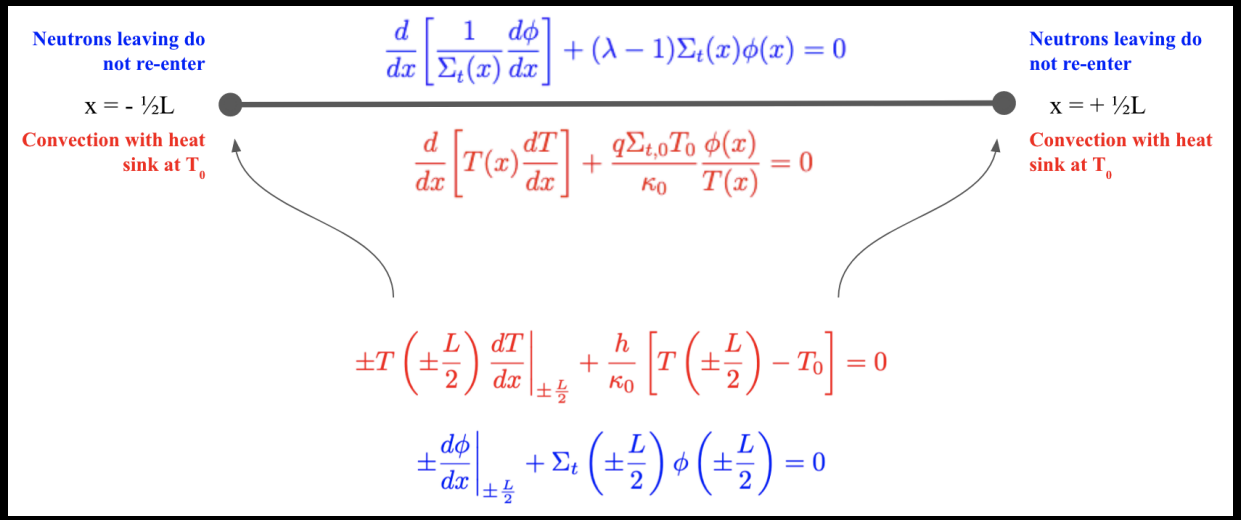

- The fundamental assumption (ansatz) of [1]: $T(x) = f\phi(x)$.
- This imposes two constraints that determine the system heat transfer coefficient h and the total microscopic cross section $\sigma_{t,0}$. The solution that satisfies the above is given by an elliptical flux shape

$$\phi(x) = \phi(0)\sqrt{1 - \frac{(\lambda - 1)P^2x^2}{L^2q^2\phi^2(0)}} \tag{7}$$

System Domain, Differential Equations, and Boundary Conditions

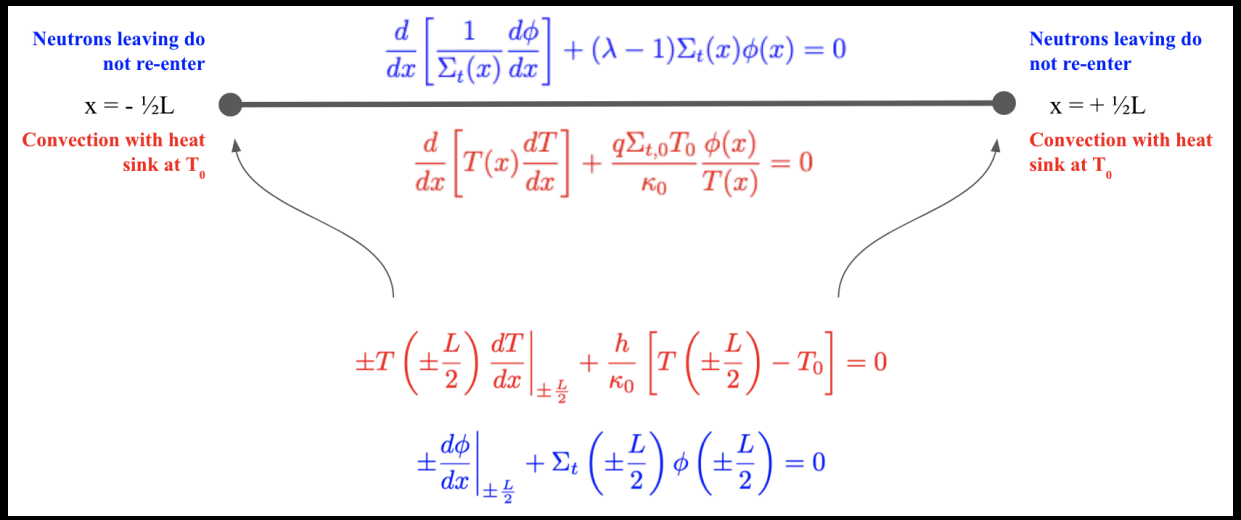

- The fundamental assumption (ansatz) of [1]: $T(x) = f\phi(x)$.
- This imposes two constraints that determine the system heat transfer coefficient h and the total microscopic cross section $\sigma_{t,0}$. The solution that satisfies the above is given by an elliptical flux shape

$$\phi(x) = \phi(0)\sqrt{1 - \frac{(\lambda - 1)P^2x^2}{L^2q^2\phi^2(0)}} \tag{7}$$

- where P is the slab power and L is the slab equilibrium length.

OpenMC Model

OpenMC Model

- Slab geometry divided into N cells, $N = [5, 10, 25, 50, 100, 250, 500, 1000]$.

OpenMC Model

- Slab geometry divided into N cells, $N = [5, 10, 25, 50, 100, 250, 500, 1000]$.
- Equilibrium length $L = 106.47$ cm in the x-direction, 1 cm in the y-direction, 1 cm in the z-direction.

OpenMC Model

- Slab geometry divided into N cells, $N = [5, 10, 25, 50, 100, 250, 500, 1000]$.
- Equilibrium length $L = 106.47$ cm in the x-direction, 1 cm in the y-direction, 1 cm in the z-direction.
  - Internal x-planes use transmissive BCs and vacuum BCs for boundary planes.

OpenMC Model

- Slab geometry divided into N cells, $N = [5, 10, 25, 50, 100, 250, 500, 1000]$.
- Equilibrium length $L = 106.47$ cm in the x-direction, 1 cm in the y-direction, 1 cm in the z-direction.
  - Internal x-planes use transmissive BCs and vacuum BCs for boundary planes.
  - Y and Z-planes reflective BCs to simulate infiniteness.

OpenMC Model

- Slab geometry divided into N cells, $N = [5, 10, 25, 50, 100, 250, 500, 1000]$.
- Equilibrium length $L = 106.47$ cm in the x-direction, 1 cm in the y-direction, 1 cm in the z-direction.
  - Internal x-planes use transmissive BCs and vacuum BCs for boundary planes.
  - Y and Z-planes reflective BCs to simulate infiniteness.
- Macroscopic XS library via OpenMC's `XSData` class.

OpenMC Model

- Slab geometry divided into N cells, $N = [5, 10, 25, 50, 100, 250, 500, 1000]$.
- Equilibrium length $L = 106.47$ cm in the x-direction, 1 cm in the y-direction, 1 cm in the z-direction.
  - Internal x-planes use transmissive BCs and vacuum BCs for boundary planes.
  - Y and Z-planes reflective BCs to simulate infiniteness.
- Macroscopic XS library via OpenMC's `XSData` class.
- This temperature XS library accounts for changes in density due to temperature and uses the same mesh instead of modeling thermal expansion via a deformed mesh. Though this is possible in Cardinal [6]

OpenMC Model

- Slab geometry divided into N cells, $N = [5, 10, 25, 50, 100, 250, 500, 1000]$.
- Equilibrium length $L = 106.47$ cm in the x-direction, 1 cm in the y-direction, 1 cm in the z-direction.
  - Internal x-planes use transmissive BCs and vacuum BCs for boundary planes.
  - Y and Z-planes reflective BCs to simulate infiniteness.
- Macroscopic XS library via OpenMC's `XSData` class.
- This temperature XS library accounts for changes in density due to temperature and uses the same mesh instead of modeling thermal expansion via a deformed mesh. Though this is possible in Cardinal [6]
- Library has data for every integer temperature between 308 K and 358 K and rounds to nearest for a lookup between two data points.

OpenMC Model

- Slab geometry divided into N cells, $N = [5, 10, 25, 50, 100, 250, 500, 1000]$.
- Equilibrium length $L = 106.47$ cm in the x-direction, 1 cm in the y-direction, 1 cm in the z-direction.
  - Internal x-planes use transmissive BCs and vacuum BCs for boundary planes.
  - Y and Z-planes reflective BCs to simulate infiniteness.
- Macroscopic XS library via OpenMC's `XSData` class.
- This temperature XS library accounts for changes in density due to temperature and uses the same mesh instead of modeling thermal expansion via a deformed mesh. Though this is possible in Cardinal [6]
- Library has data for every integer temperature between 308 K and 358 K and rounds to nearest for a lookup between two data points.
- Library uses one energy group from 0 to 20 MeV.

OpenMC Model

- Slab geometry divided into N cells, $N = [5, 10, 25, 50, 100, 250, 500, 1000]$.
- Equilibrium length $L = 106.47$ cm in the x-direction, 1 cm in the y-direction, 1 cm in the z-direction.
  - Internal x-planes use transmissive BCs and vacuum BCs for boundary planes.
  - Y and Z-planes reflective BCs to simulate infiniteness.
- Macroscopic XS library via OpenMC's `XSData` class.
- This temperature XS library accounts for changes in density due to temperature and uses the same mesh instead of modeling thermal expansion via a deformed mesh. Though this is possible in Cardinal [6]
- Library has data for every integer temperature between 308 K and 358 K and rounds to nearest for a lookup between two data points.
- Library uses one energy group from 0 to 20 MeV.
- S_2 patch to restrict particle birth direction and scattering direction to only $\pm$x.

OpenMC Model

- Slab geometry divided into N cells, $N = [5, 10, 25, 50, 100, 250, 500, 1000]$.
- Equilibrium length $L = 106.47$ cm in the x-direction, 1 cm in the y-direction, 1 cm in the z-direction.
  - Internal x-planes use transmissive BCs and vacuum BCs for boundary planes.
  - Y and Z-planes reflective BCs to simulate infiniteness.
- Macroscopic XS library via OpenMC's `XSData` class.
- This temperature XS library accounts for changes in density due to temperature and uses the same mesh instead of modeling thermal expansion via a deformed mesh. Though this is possible in Cardinal [6]
- Library has data for every integer temperature between 308 K and 358 K and rounds to nearest for a lookup between two data points.
- Library uses one energy group from 0 to 20 MeV.
- S_2 patch to restrict particle birth direction and scattering direction to only $\pm$x.
- Tallies flux and kappa-fission heating rate.

MOOSE Heat Conduction Model

MOOSE Heat Conduction Model

- Mesh with identical dimensions as OpenMC model. Allows 1:1 feedback between single physics solves.

MOOSE Heat Conduction Model

- Mesh with identical dimensions as OpenMC model. Allows 1:1 feedback between single physics solves.
- MOOSE accepts heating rate in each mesh element from OpenMC and solves for temperature distribution.

MOOSE Heat Conduction Model

- Mesh with identical dimensions as OpenMC model. Allows 1:1 feedback between single physics solves.
- MOOSE accepts heating rate in each mesh element from OpenMC and solves for temperature distribution.
- Convective boundary conditions at end points with heat since temperature T_0.

MOOSE Heat Conduction Model

- Mesh with identical dimensions as OpenMC model. Allows 1:1 feedback between single physics solves.
- MOOSE accepts heating rate in each mesh element from OpenMC and solves for temperature distribution.
- Convective boundary conditions at end points with heat since temperature T_0.
- Jacobi Free Newton Krylov solver: 10^{-7} absolute tolerance and 10^{-9} relative tolerance

Coupling, Data Mapping, and Convergence Criteria

Coupling, Data Mapping, and Convergence Criteria

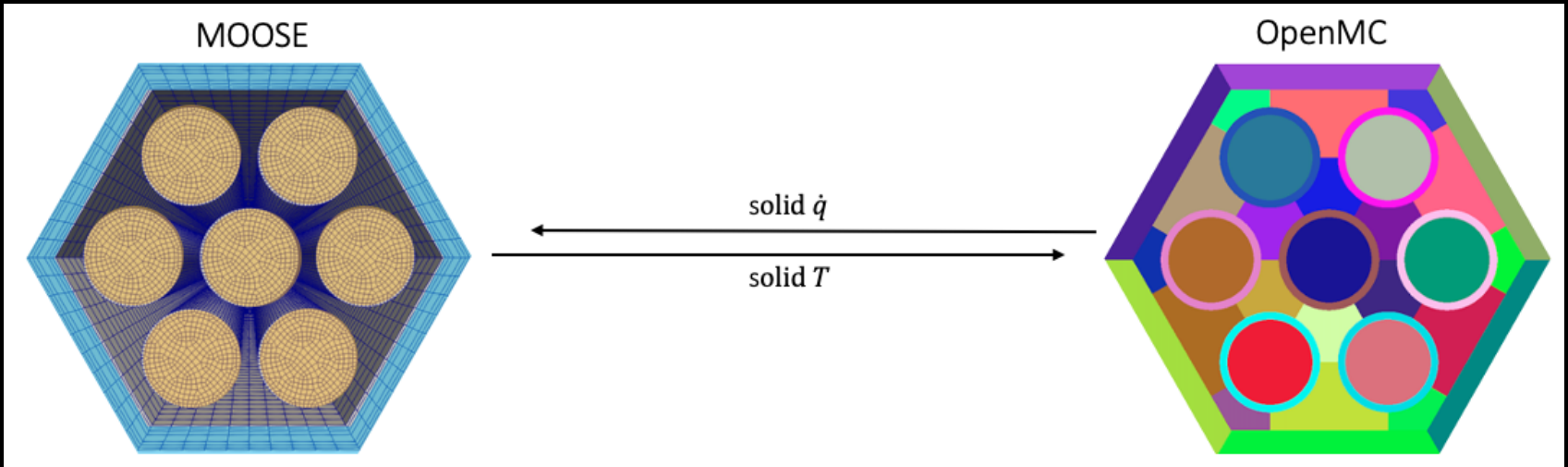

Coupling, Data Mapping, and Convergence Criteria

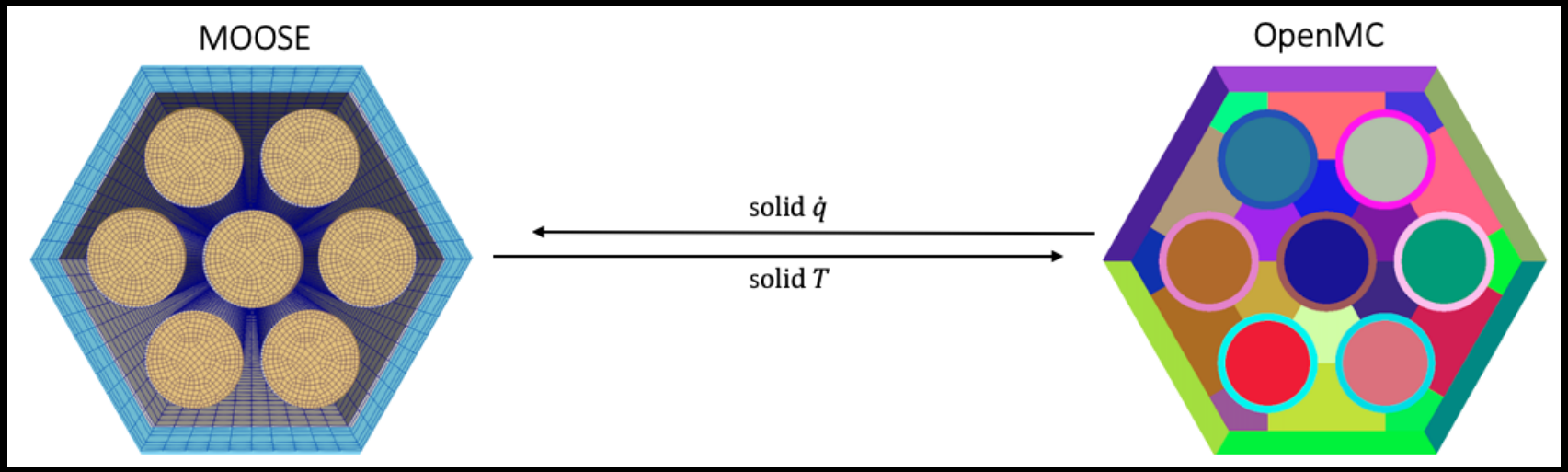

- 200 Picard Iterations. Robbins-Monro relaxation assisted tally statistics [7].

Coupling, Data Mapping, and Convergence Criteria

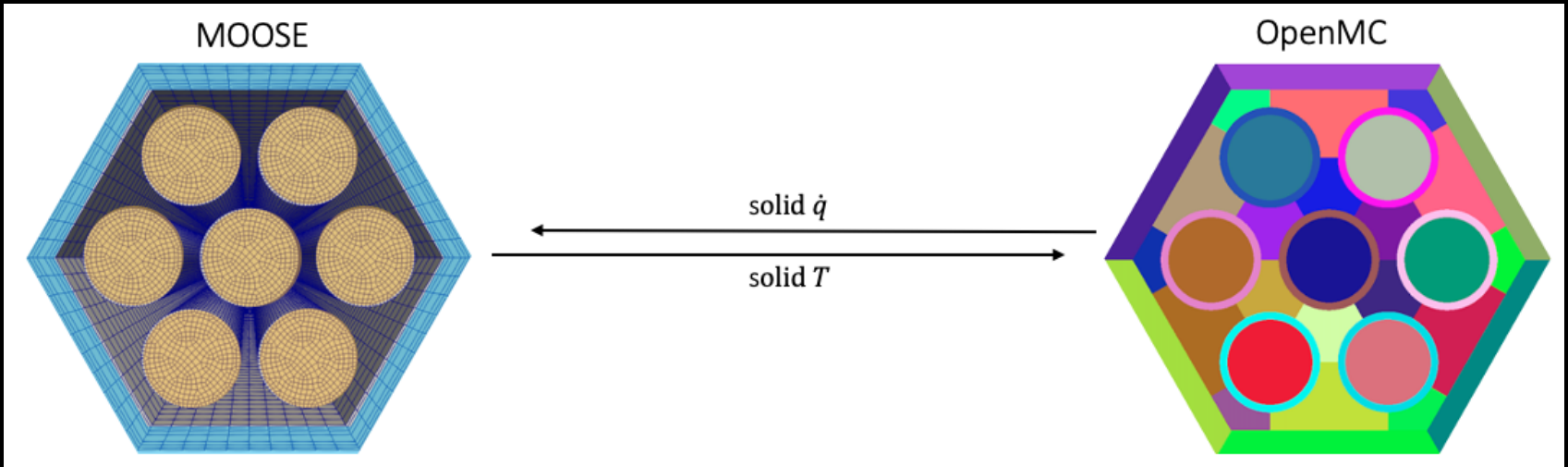

- 200 Picard Iterations. Robbins-Monro relaxation assisted tally statistics [7].
- k-eigenvalue simulation used 50,000 particles per batch, 50 inactive batches and 100 active batches.

Coupling, Data Mapping, and Convergence Criteria

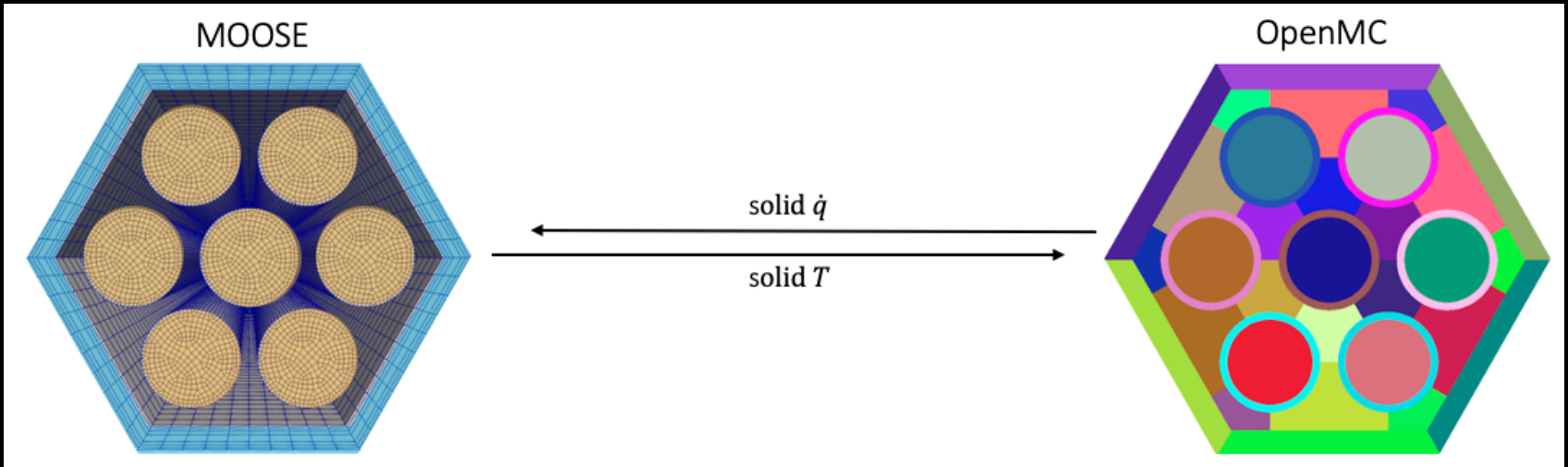

- 200 Picard Iterations. Robbins-Monro relaxation assisted tally statistics [7].
- k-eigenvalue simulation used 50,000 particles per batch, 50 inactive batches and 100 active batches.
  - Shannon Entropy study confirmed this sufficient following criteria from [8].

Coupling, Data Mapping, and Convergence Criteria

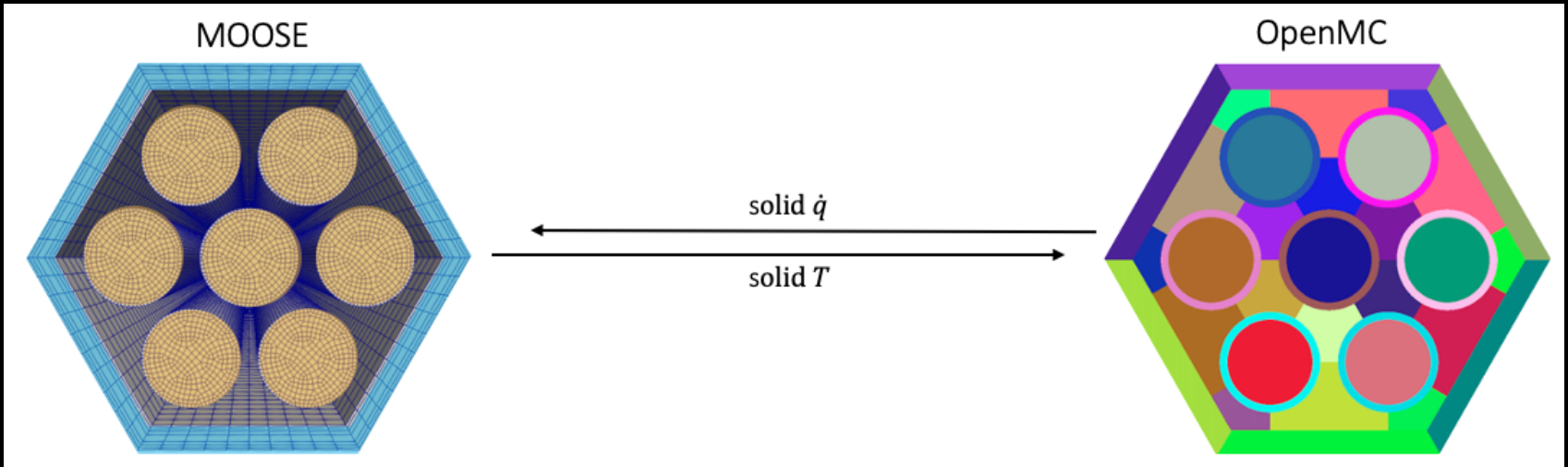

- 200 Picard Iterations. Robbins-Monro relaxation assisted tally statistics [7].
- k-eigenvalue simulation used 50,000 particles per batch, 50 inactive batches and 100 active batches.
  - Shannon Entropy study confirmed this sufficient following criteria from [8].
- Final transport solve with converged temperature used 250,000 particles per batch.

Outputs and Comparisons

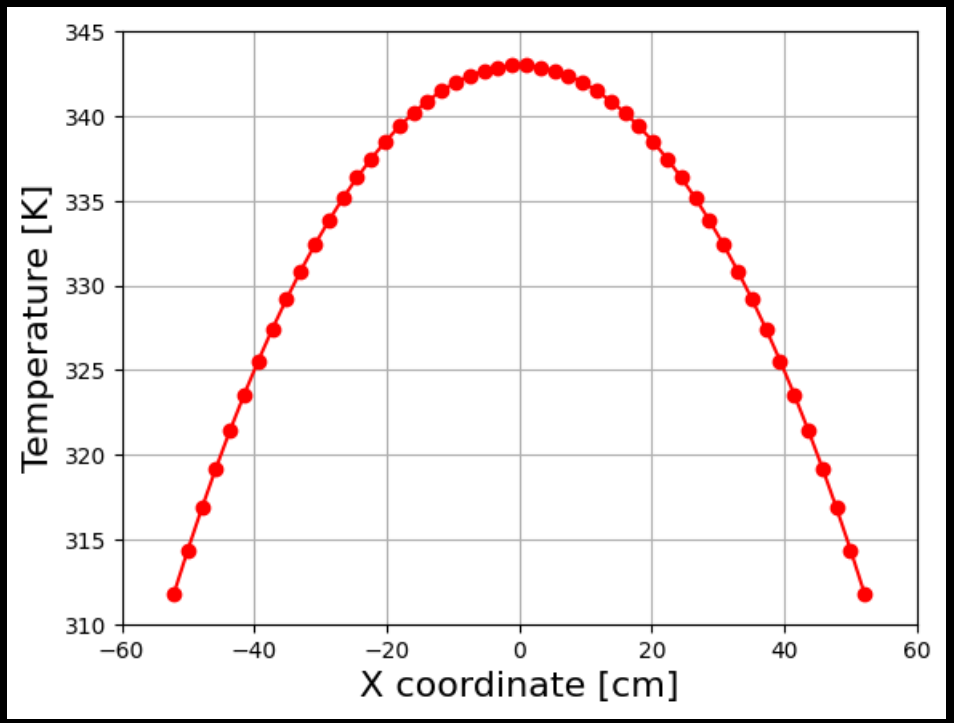

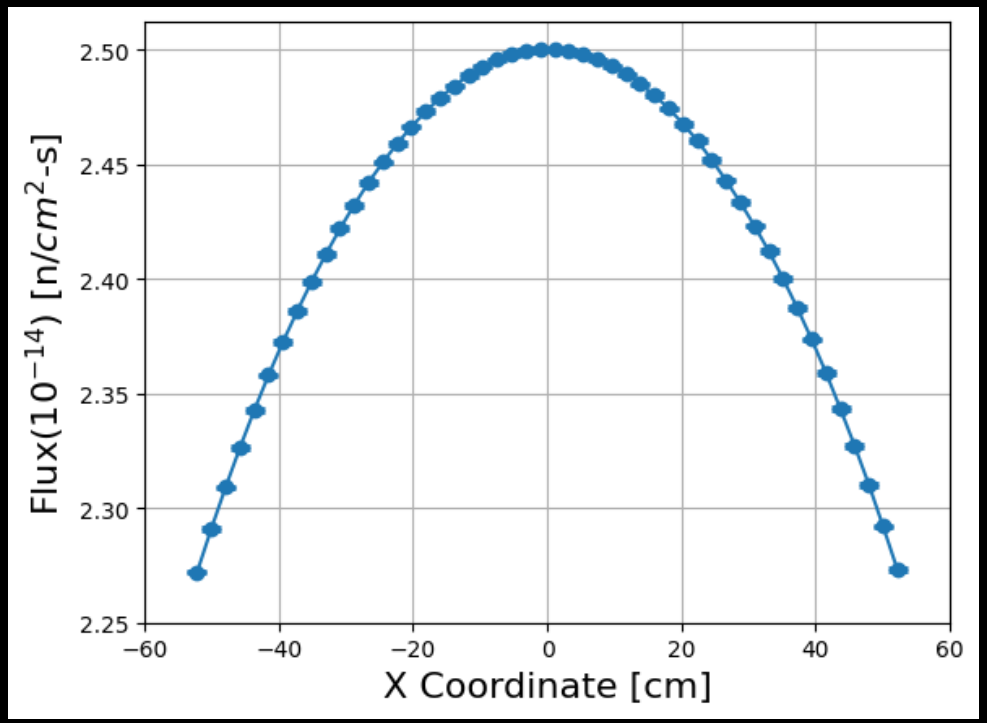

- Numerical solutions for 50 mesh elements. On the right, error bars show the relative error of the flux, which are nearly smaller than the circular marker sizes.

Solution L_2 Error Norms

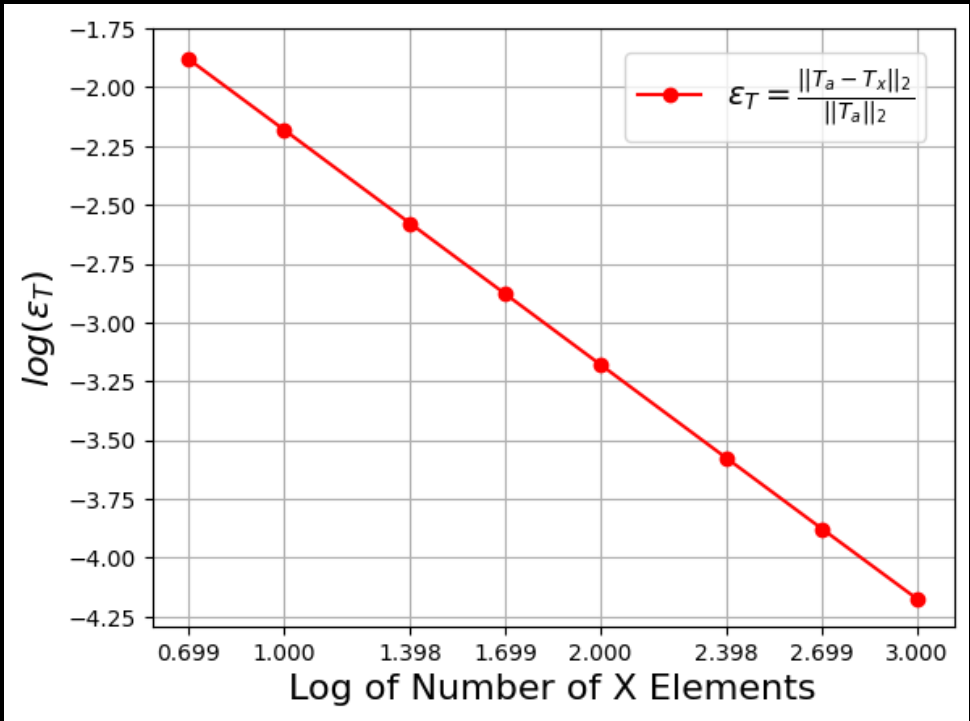

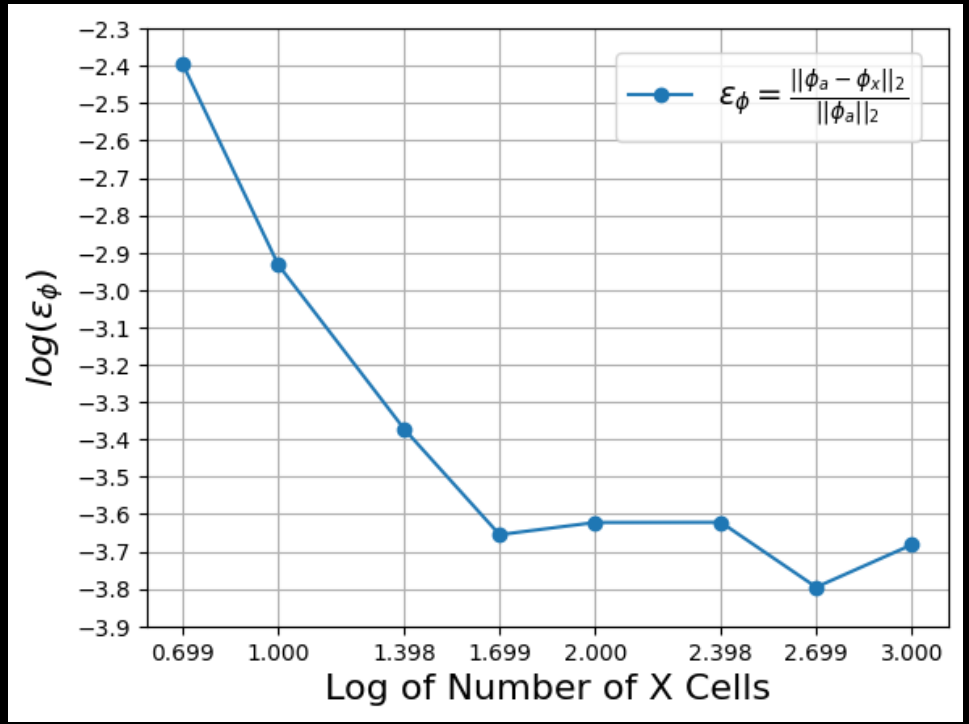

- Error norms as a function of heat conduction mesh element count and OpenMC cell count, respectively.

Computed to Expected Ratios

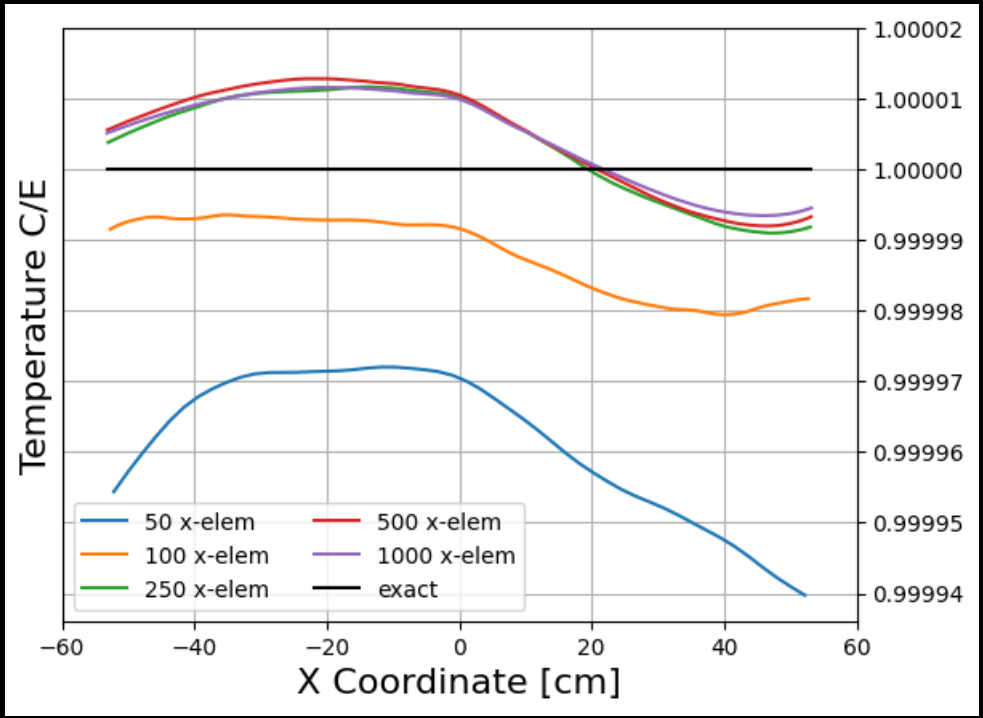

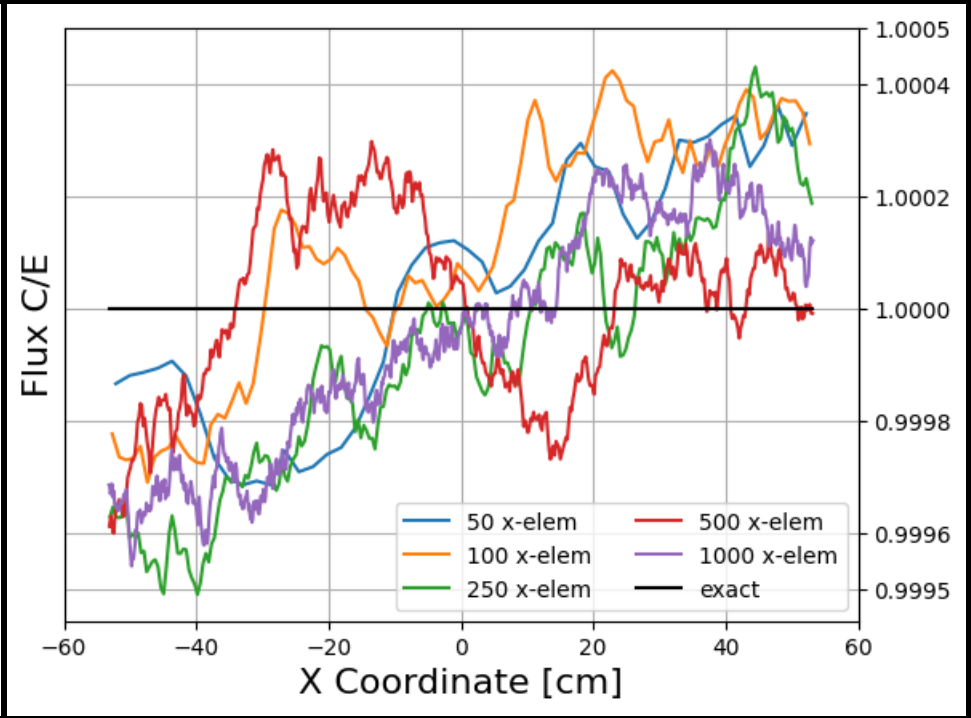

- C/E for fine cases ($N = 50, 100, 250, 500, 1000$). Note the scales of the y-axes - the temperature is everywhere being predicted to within 0.006% (for the coarsest shown temperature mesh) and flux is everywhere being predicted to within 0.05%.

Individual Flux C/E with 2σ Error Bars for Fine Cases

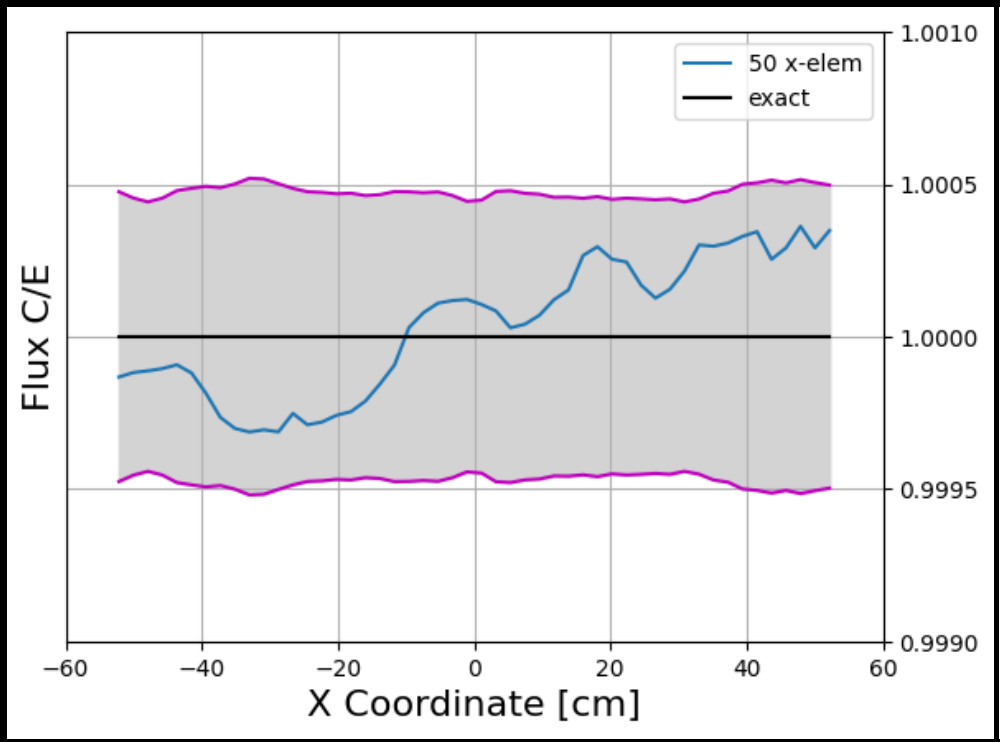

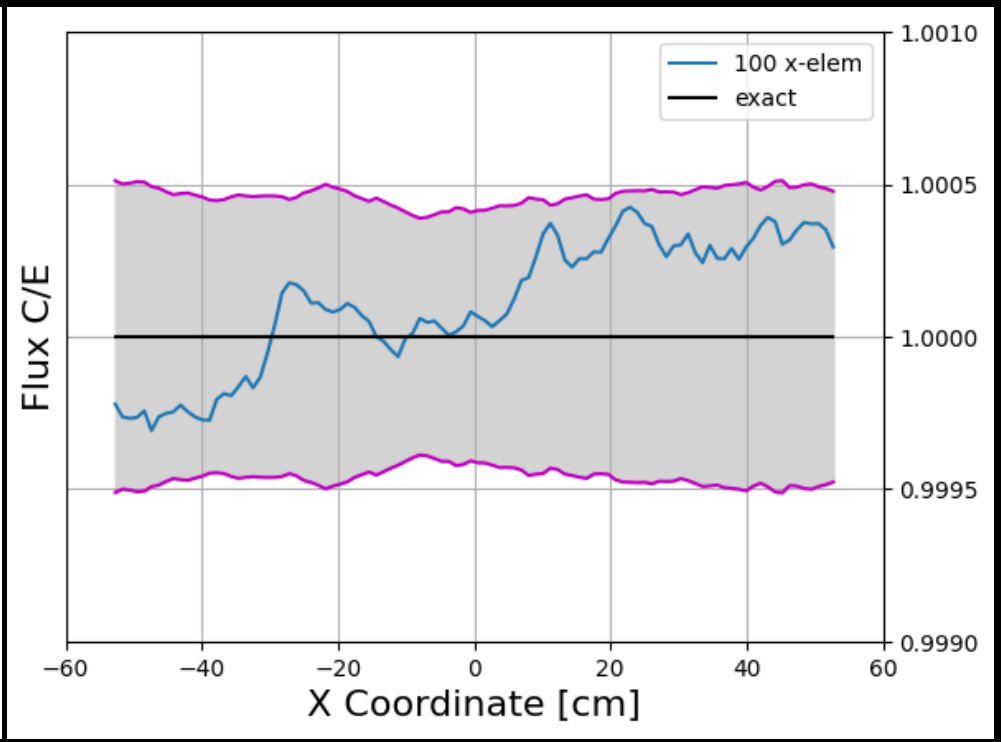

- C/E in blue with 2σ error bars (gray bounded by purple). 50 and 100 cells.

Individual Flux C/E with 2σ Error Bars for Fine Cases

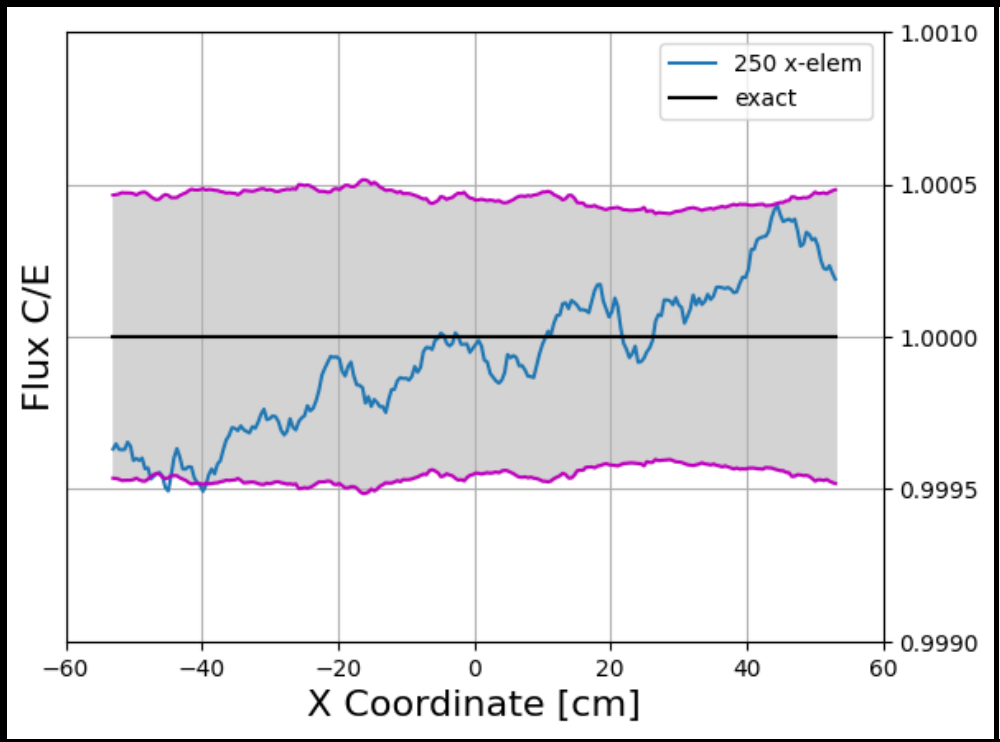

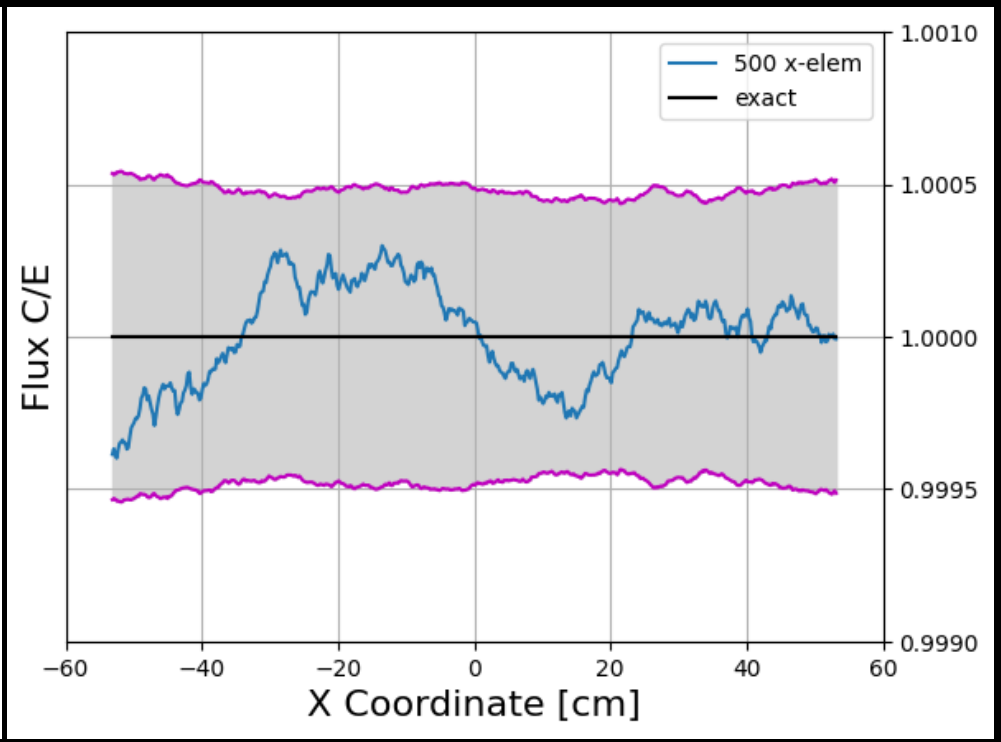

- C/E in blue with 2σ error bars (gray bounded by purple). 250 and 500 cells

Individual Flux C/E with 2σ Error Bars for Fine Cases

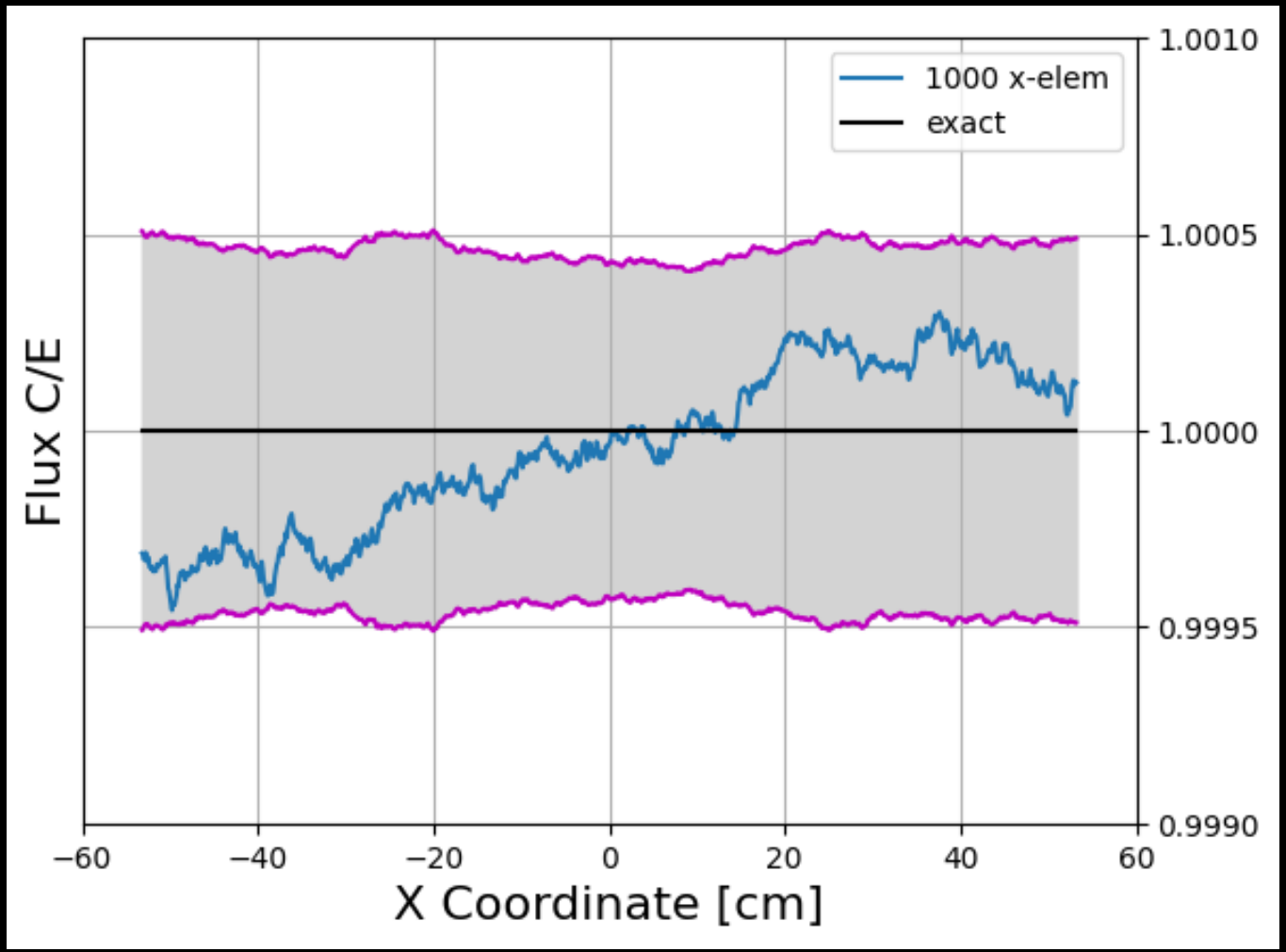

Future and companion work

- discuss using nek, mention [9]

Bibliography

[1] D.P. Griesheimer and G. Kooreman. "Analytical Benchmark Solution for 1-D Neutron Transport Coupled with Thermal Conduction and Material Expansion". In: *Proceedings of M&C*. Pittsburgh, Pennsylvania, 2022.

[2] A.J. Novak et al. "Coupled Monte Carlo and Thermal-Fluid Modeling of High Temperature Gas Reactors Using Cardinal". In: *Annals of Nuclear Energy* 177 (2022), p. 109310. DOI: 10.1016/j.anucene.2022.109310.

[3] P.K. Romano et al. "OpenMC: A State-of-the-Art Monte Carlo Code for Research and Development". In: *Annals of Nuclear Energy* 82 (2015), pp. 90–97. DOI: 10.1016/j.anucene.2014.07.048.

[4] P. Fischer et al. *NekRS, a GPU-Accelerated Spectral Element Navier-Stokes Solver*. arXiv:2104.05829. Apr. 2021.

[5] Alexander D. Lindsay et al. "2.0 - MOOSE: Enabling massively parallel multiphysics simulation". In: *SoftwareX* 20 (2022), p. 101202. ISSN: 2352-7110. DOI: https://doi.org/10.1016/j.softx.2022.101202.

[6] A.J. Novak et al. "Multiphysics Coupling of OpenMC CAD-Based Transport to MOOSE using Cardinal and Aurora". In: *Proceedings of M&C*. Niagara Falls, Ontario, Canada, 2023.

Bibliography

[7] J. Dufek and W. Gudowski. "Stochastic Approximation for Monte Carlo Calculation of Steady-State Conditions in Thermal Reactors". In: *Nuclear Science and Engineering* 152 (2006), pp. 274–283. DOI: 10.13182/NSE06-2.

[8] F.B. Brown. "On the Use of Shannon Entropy of the Fission Distribution for Assessing Convergence of Monte Carlo Criticality Calculations". In: *Proceedings of PHYSOR*. Vancouver, British Columbia, Canada, 2006.

[9] A.H. Hegazy and A.J. Novak. "Verification of the Cardinal Multiphysics Solver with the Doppler Slab Benchmark". In: *Proceedings of M&C*. Niagara Falls, Ontario, Canada, 2023.

Acknowledgements

- Benchmark authors: David P. Greisheimer and Gabriel Kooreman
- Co-authors: April J. Novak, Patrick Shriwise, Paul P.H. Wilson
- OpenMC, Cardinal, and MOOSE teams!

Coarse C/E results

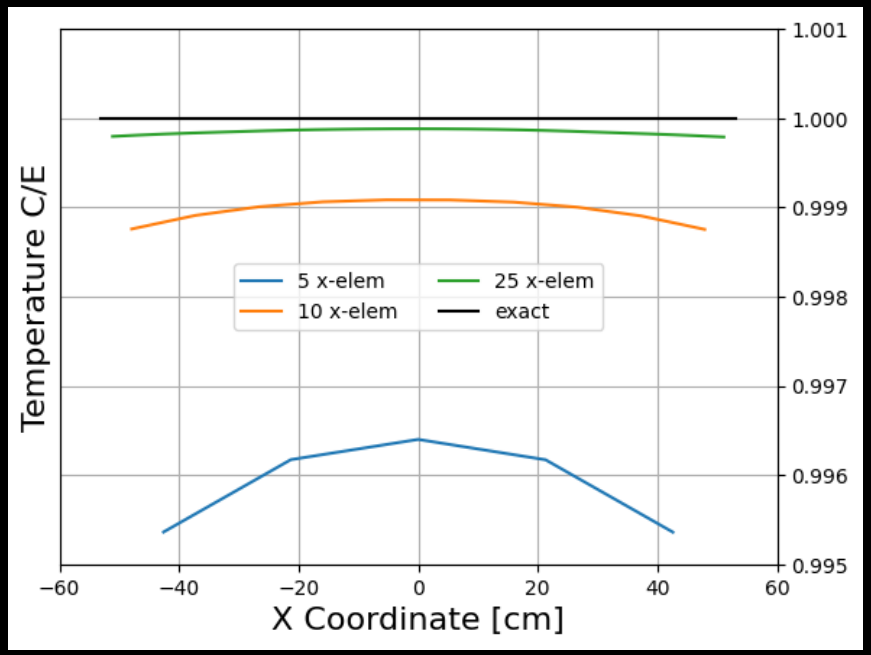

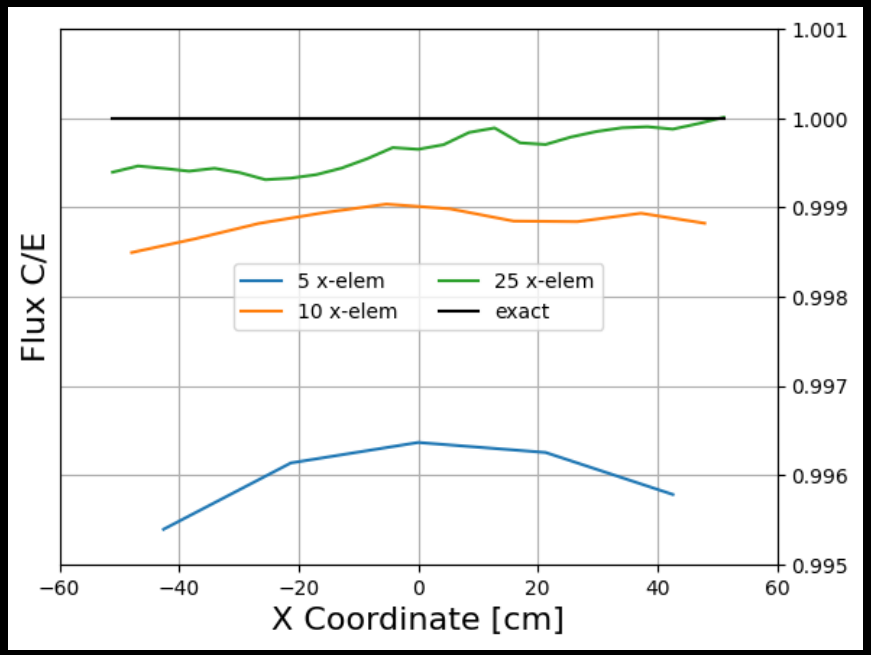

- C/E for coarse cases ($N = 5, 10, 25$). The coarse cases' errors are a few orders of magnitude larger than the fine cases. A significant improvement in agreement can be seen between each coarse case.

Ensuring Validity of the Fundamental Ansatz

- Taking the heat conduction ODE

$$\frac{d}{dx}\left[\kappa(T(x))\frac{dT(x)}{dx}\right] + q\Sigma_t(x)\phi(x) = 0 \tag{8}$$

- and using the thermal conductivity and cross section temperature dependence

$$\frac{d}{dx}\left[\kappa_0 T(x)\frac{dT(x)}{dx}\right] + q\Sigma_{t,0}\frac{T_0}{T(x)}\phi(x) = 0 \tag{9}$$

- Taking the neutron transport ODE

$$\frac{d}{dx}\left[\frac{1}{\Sigma_t(x)}\frac{d\phi(x)}{dx}\right] + \Sigma_t(x)\left(\lambda - 1\right)\phi(x) = 0 \tag{10}$$

- and inserting cross section temperature dependence gives

$$\frac{d}{dx}\left[\frac{T(x)}{\Sigma_{t,0}T_0}\frac{d\phi(x)}{dx}\right] + \Sigma_{t,0}\frac{T_0}{T(x)}\left(\lambda - 1\right)\phi(x) = 0 \tag{11}$$

Ensuring Validity of the Fundamental Ansatz

- these two equations are very close, and after some re-arranging, they look even closer

$$\frac{d}{dx}\left[T(x)\frac{dT(x)}{dx}\right] + \frac{q\Sigma_{t,0}}{\kappa_0}\frac{T_0}{T(x)}\phi(x) = 0 \qquad \text{AND}$$

$$\frac{d}{dx}\left[\frac{T(x)}{\Sigma_{t,0}T_0}\frac{d\phi(x)}{dx}\right] + \Sigma_{t,0}\frac{T_0}{T(x)}(\lambda - 1)\phi(x) = 0 \quad (12)$$

- Applying the ansatz $T(x) = f\phi(x)$ gives

$$\frac{d}{dx}\left[f^2\phi(x)\frac{d\phi(x)}{dx}\right] + \frac{q\Sigma_{t,0}}{\kappa_0}\frac{T_0}{f} = 0 \qquad \text{AND}$$

$$\frac{d}{dx}\left[\frac{f\phi(x)}{\Sigma_{t,0}T_0}\frac{d\phi(x)}{dx}\right] + \Sigma_{t,0}\frac{T_0}{f}(\lambda - 1) = 0 \quad (13)$$

$$\frac{d}{dx}\left[\phi(x)\frac{d\phi(x)}{dx}\right] + \frac{q\Sigma_{t,0}}{\kappa_0}\frac{T_0}{f^3} = 0 \qquad \text{AND}$$

$$\frac{d}{dx}\left[\phi(x)\frac{d\phi(x)}{dx}\right] + \left(\Sigma_{t,0}\frac{T_0}{f}\right)^2(\lambda - 1) = 0 \quad (14)$$

Ensuring Validity of the Fundamental Ansatz

- In order to make the ansatz hold, this implies that

$$\frac{q\Sigma_{t,0}}{\kappa_0}\frac{T_0}{f^3} = \left(\Sigma_{t,0}\frac{T_0}{f}\right)^2(\lambda-1) \qquad \text{OR} \qquad \Sigma_{t,0} = \frac{q}{(\lambda-1)\kappa_0 T_0 f} \tag{15}$$

  which is a condition for the total cross section based on system parameters.

- A similar process of matching coefficients must be applied to the boundary conditions to gain a condition for the heat transfer coefficient. Though, at this point, realize that

$$\frac{d}{dx}\left[\phi(x)\frac{d\phi(x)}{dx}\right] + \left(\Sigma_{t,0}\frac{T_0}{f}\right)^2(\lambda-1) = 0 \tag{16}$$

- is a separable ODE that can be solved for an analytical solution. The result for the heat transfer coefficient is given by

$$h\left(\sqrt{\frac{L(\lambda-1)}{\kappa_0 P}} - \frac{2T_0}{P}\right) = 1 \tag{17}$$

Deriving the Benchmark ODE for $\phi(x)$

- Going from the steady-state, mono-energetic, 1-D neutron transport equation to the ODE that describes neutron transport for this benchmark:

$$\mu \frac{\partial \psi(x,\mu)}{\partial x} + \Sigma_t(x)\psi(x,\mu) = \int_{-1}^{1} \frac{1}{2}\left[\Sigma_s(x) + \frac{\nu\Sigma_f(x)}{k_{eff}}\right]\psi(x,\mu')d\mu' \tag{18}$$

For now, lump the fission term into the scattering cross section to get

$$\mu \frac{\partial \psi(x,\mu)}{\partial x} + \Sigma_t(x)\psi(x,\mu) = \int_{-1}^{1} \frac{1}{2}\Sigma_s(x)\psi(x,\mu')d\mu' \tag{19}$$

Define the scalar flux and the magnitude of current

$$\phi(x) = \int_{-1}^{1} \psi(x,\mu)d\mu \qquad \text{AND} \qquad J(x) = \int_{-1}^{1} \mu\psi(x,\mu)d\mu. \tag{20}$$

Considering S_2 transport means restricting the angular cosine to $\mu = \pm 1$:

$$\psi(x,\mu) = \psi(x,-1)\delta(\mu+1) + \psi(x,1)\delta(\mu-1) \tag{21}$$

(sometimes denoted $\psi^+ \equiv \psi(x,1)\delta(\mu-1)$ and $\psi^- \equiv \psi(x,-1)\delta(\mu+1)$)

Deriving the Benchmark ODE for $\phi(x)$

Now carrying out the integral definitions with S_2 quantities gives

$$\phi(x) = \int_{-1}^{1} \left[\psi(x,-1)\delta(\mu+1) + \psi(x,1)\delta(\mu-1)\right] d\mu = \psi(x,-1) + \psi(x,1) \tag{22}$$

and

$$J(x) = \int_{-1}^{1} \mu \left[\psi(x,-1)\delta(\mu+1) + \psi(x,1)\delta(\mu-1)\right] d\mu = \psi(x,1) - \psi(x,-1) \tag{23}$$

Evaluating (19) at $\mu = \pm 1$ gives

$$-\frac{\partial \psi(x,-1)}{\partial x} + \Sigma_t(x)\psi(x,-1) = \frac{1}{2}\Sigma_s(x)\phi(x); \tag{24}$$

$$\frac{\partial \psi(x,1)}{\partial x} + \Sigma_t(x)\psi(x,1) = \frac{1}{2}\Sigma_s(x)\phi(x). \tag{25}$$

Adding (24) and (25) gives

$$-\frac{\partial \psi(x,-1)}{\partial x} + \frac{\partial \psi(x,1)}{\partial x} + \Sigma_t(x)\left(\psi(x,-1) + \psi(x,1)\right) = \Sigma_s(x)\phi(x) \tag{26}$$

Deriving the Benchmark ODE for $\phi(x)$

The results for $\phi(x)$ and $J(x)$ can simplify (26)

$$\frac{dJ(x)}{dx} + \Sigma_t(x)\phi(x) = \Sigma_s(x)\phi(x) \tag{27}$$

Subtracting (24) and (25) gives

$$-\frac{\partial\psi(x,-1)}{dx} - \frac{\partial\psi(x,1)}{dx} + \Sigma_t(x)\left(\psi(x,-1) - \Sigma_t(x)\psi(x,1)\right) = 0 \tag{28}$$

Which can be transformed with similar tricks to

$$\frac{d\phi(x)}{dx} + \Sigma_t(x)J(x) = 0 \qquad \text{OR} \qquad J(x) = -\frac{1}{\Sigma_t(x)}\frac{d\phi(x)}{dx} \tag{29}$$

Since $\frac{dJ(x)}{dx}$ appears in (27), we can take the derivative of both sides of (29) and substitute it in

$$\frac{dJ(x)}{dx} = -\frac{d}{dx}\left[\frac{1}{\Sigma_t(x)}\frac{d\phi(x)}{dx}\right] \tag{30}$$

Now the equation that only depends on $\phi(x)$ is given by

$$-\frac{d}{dx}\left[\frac{1}{\Sigma_t(x)}\frac{d\phi(x)}{dx}\right] + \Sigma_t(x)\phi(x) = \Sigma_s(x)\phi(x) \tag{31}$$

Deriving the Benchmark ODE for $\phi(x)$

At this point, we "un-lump" the scattering cross section to write out the fission term

$$-\frac{d}{dx}\left[\frac{1}{\Sigma_t(x)}\frac{d\phi(x)}{dx}\right]+\Sigma_t(x)\phi(x)=\left[\Sigma_s(x)+\frac{\nu\Sigma_f}{k_{eff}}\right]\phi(x) \tag{32}$$

$$-\frac{d}{dx}\left[\frac{1}{\Sigma_t(x)}\frac{d\phi(x)}{dx}\right]+\Sigma_t(x)\left[1-\frac{\Sigma_s(x)+\frac{\nu\Sigma_f}{k_{eff}}}{\Sigma_t}\right]\phi(x)=0 \tag{33}$$

$$\frac{d}{dx}\left[\frac{1}{\Sigma_t(x)}\frac{d\phi(x)}{dx}\right]+\Sigma_t(x)\left[\frac{\Sigma_s(x)+\frac{\nu\Sigma_f}{k_{eff}}}{\Sigma_t}-1\right]\phi(x)=0 \tag{34}$$

Now define

$$\lambda\equiv\frac{\Sigma_s(x)+\frac{\nu\Sigma_f}{k_{eff}}}{\Sigma_t} \tag{35}$$

giving the final result:

$$\frac{d}{dx}\left[\frac{1}{\Sigma_t(x)}\frac{d\phi(x)}{dx}\right]+\Sigma_t(x)\left(\lambda-1\right)\phi(x)=0 \tag{36}$$

Deriving the Benchmark ODE for $\phi(x)$

The next task is to apply boundary conditions so that $\phi(x)$ can be specified. In discrete ordinates with $\mu = \pm 1$ (S_2), we use the vacuum boundary condition. The angular flux for positive angular cosines is zero at the left boundary and is zero for negative angular cosines at the right boundary. Using the previous results for $\phi(x)$ and $J(x)$ at the boundaries gives

$$\phi(x = \frac{L}{2}) = \psi(x = \frac{L}{2}, \mu = -1) + \psi(x = \frac{L}{2}, \mu = 1) \quad \text{AND}$$
$$\phi(x = -\frac{L}{2}) = \psi(x = -\frac{L}{2}, \mu = -1) + \psi(x = -\frac{L}{2}, \mu = 1) \quad (37)$$

and

$$J(x = \frac{L}{2}) = -\psi(x = \frac{L}{2}, -1) + \psi(x = \frac{L}{2}, 1) \quad \text{AND}$$
$$J(x = -\frac{L}{2}) = -\psi(x = -\frac{L}{2}, -1) + \psi(x = -\frac{L}{2}, 1) \quad (38)$$

Deriving the Benchmark ODE for $\phi(x)$

Now, terms can be crossed out due to vacuum boundaries. This gives that

$$\phi(x = \frac{L}{2}) = \psi(x = \frac{L}{2}, \mu = 1) \qquad \text{AND}$$

$$\phi(x = -\frac{L}{2}) = \psi(x = -\frac{L}{2}, \mu = -1) \tag{39}$$

$$J(x = \frac{L}{2}) = \psi(x = \frac{L}{2}, \mu = 1) \qquad \text{AND}$$

$$J(x = -\frac{L}{2}) = -\psi(x = -\frac{L}{2}, \mu = -1) \tag{40}$$

Using this with (29) gives the desired boundary conditions

$$J(x = \pm\frac{L}{2}) = \pm\phi(x = \pm\frac{L}{2}) \tag{41}$$

And the boundary conditions of interest are now

$$\left.\frac{d\phi}{dx}\right|_{x=\pm\frac{L}{2}} \pm \Sigma_t(x = \pm\frac{L}{2})\phi(x = \pm\frac{L}{2}) = 0 \tag{42}$$